Electronic Supplementary Material (ESI) for Inorganic Chemistry Frontiers.
This journal is © the Partner Organisations 2023

Electronic Supplementary Information

Experiment Section

Materials: Titanium plate (0.4 mm in thickness) was purchased from Qingyuan Metal Materials Co., Ltd (Xingtai, China). Sodium hydroxide (NaOH), sodium nitrate ($NaNO_3$), sodium nitrite ($NaNO_2$), salicylic acid, sodium citrate, ruthenium(III) chloride trihydrate ($RuCl_3 \cdot 3H_2O$), and ethanol were bought from Beijing Chemical Corporation (China). Ruthenium oxide (RuO_2), Nafion (5 wt%), 5,5-dimethyl-1-pyrroline-N-oxide (DMPO), sodium chloride (NaCl), sulfanilamide, sodium nitroferricyanide dihydrate, sodium sulphate (Na_2SO_4), and perchloric acid ($HClO_4$) were obtained from Aladdin Reagent (Shanghai, China). Phosphoric acid (H_3PO_4), hydrochloric acid (HCl), nitric acid (HNO_3), and N-(1-naphthyl)ethylenediamine dihydrochloride were bought from Keshi Chemical Reagent Co. All chemicals were used as received without further purification.

Preparation of RuO_2@TiO_2/TP: Firstly, Ti plate (TP) (2.0 × 4.0 cm^2) was immersed in concentrated HCl at 70 °C for 15 min and then ultrasonicated in ethanol and water for 10 min, respectively. The pre-tread TP was put into a Teflon-lined autoclave containing 40 mL of 5 M NaOH solution, and then the autoclave was kept in an electric oven at 180 °C for 24 h. After natural cooling of the autoclave, the sample was moved out, washed several times with deionized water and ethanol, and dried at 60 °C for 30 min. Then the sample was immersed in 0.25 M $RuCl_3 \cdot 3H_2O$ for 30 min to exchange Na^+ with Ru^{3+}. Subsequently, Ru-titanate/TP was annealed in a muffle

furnace at 450 °C for 3 h at a rate of 5 °C min^{-1} under air atmosphere. After cooling to room temperature, RuO_2@TiO_2/TP was finally obtained.

Electrochemical tests: All electrochemical measurements were conducted using CHI 660E (CH Instruments, China). The prepared sample (0.5 × 0.5 cm^2), graphite rod, and saturated calomel electrode (SCE) were used as working electrode, counter electrode, and reference electrode, respectively. Unless otherwise stated, all the potentials in this experiment are presented as RHE: E (vs. RHE) = E (vs. Hg/HgO) + 0.0591 × pH + 0.24. Electrochemical impedance spectroscopy (EIS) tests were performed at different applied potentials in the frequency range of 0.01 – 100000 Hz with a potential amplitude of 5 mV.

Characterizations: The phase and composition of the samples were obtained by X-ray diffraction (XRD, Philip D8) and X-ray photoelectron spectroscopy (XPS, ESCALAB 250 Xi). The morphology of the samples was investigated by scanning electron microscopy (SEM, ZISS 300) and transmission electron microscopy (TEM, JEM-F200, JEOL Ltd.). The loading of RuO_2 in RuO_2-TiO_2/Ti was performed by inductively coupled plasma-mass spectrometry (ICP-MS). The sample preparation was made by dissolving a piece of 0.5 × 0.5 cm^2 sample in 1 mL of concentrated HNO_3 and 3 mL of concentrated HCl solution. Solutions were heated at 50 °C in a sonication bath. The loading of RuO_2 in RuO_2@TiO_2/Ti is 1.264 × 10^{-4} mg cm^{-2}. Absorbance data were acquired on UV-vis spectrophotometer (Shimadzu UV-2700). In situ Raman measurements were performed using a Horiba-Xplora Plus confocal

microscope with 633 nm laser in ~20 mL of electrolyte. The Electron paramagnetic resonance (EPR) measurements were recorded by a Bruker EMX plus X-band EPR spectrometer. DMPO was selected as the spin trapping agent. Chronoamperometry was carried out at a given constant potential of 2.1 V for 60 s, and 100 mM DMPO was added during the reaction.

Determination of active chlorine: The yield of active chlorine in the electrolyte was measured based on the DPD colorimetric method using a UV-vis spectrophotometer. After a constant potential had been applied for 15 min, the electrolyte containing active chlorine was diluted 50 times with deionized water. Then, the DPD reagent reactive to active chlorine was added so that the electrolyte color changed into transparent pink. The concentration of active chlorine is calculated by UV-vis spectroscopy for a certain wavelength about 510 nm:

$$\text{Active chlorine yield} = [\text{active chlorine}] \times V / (70.9 \times t \times A)$$

where [active chlorine] is the mass concentration, V is the volume of the anodic reaction electrolyte, t is the electrolysis time, and A is the area of the working electrode.

$$\text{FE} = (n \times F \times c \times V) / (i \times t).$$

where n is the electrons transfer number, F is the Faraday constant, c is the calculated products concentration, V is the volume of the anodic reaction electrolyte, i is the applied current, and t is the electrolysis time.

Determination of nitrate: Firstly, a certain amount of electrolyte was taken out from the anodic reaction cell and diluted to 5 mL to the detection range. Then, 0.1 mL 1 M HCl and 0.01 mL 0.8 wt% sulfamic acid solution were added into the aforementioned

solution. The absorption spectrum was measured using a UV-vis spectrophotometer and the absorption intensities at a wavelength of 220 nm and 275 nm were recorded. The final absorbance value was calculated by this equation: $A = A_{220nm} - 2A_{275nm}$. The concentration-absorbance curve was calibrated using a series of standard $NaNO_3$ solutions and the $NaNO_3$ crystal was dried at 105 – 110 ºC for 2 h in advance.

Determination of nitrite: The nitrite concentration was detected by the Griess test using UV spectrophotometry. The Griess reagent was provided through adding N-(1-naphthyl)ethylenediamine dihydrochloride (0.1 g), sulfanilamide (1.0 g), and H_3PO_4 (2.94 mL) in 50 mL H_2O. Typically, 1.0 mL Griess reagent was added to 1.0 mL electrolyte and 2.0 mL H_2O. After maintained for 10 min, the concentration of nitrite was measured by UV-vis spectroscopy at a wavelength of 540 nm.

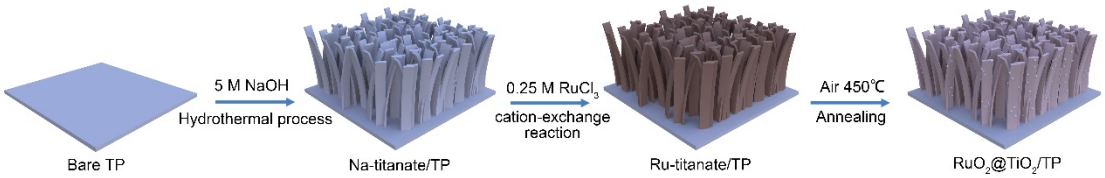

Fig. S1. Schematic illustration of the preparation process of RuO_2@TiO_2/TP.

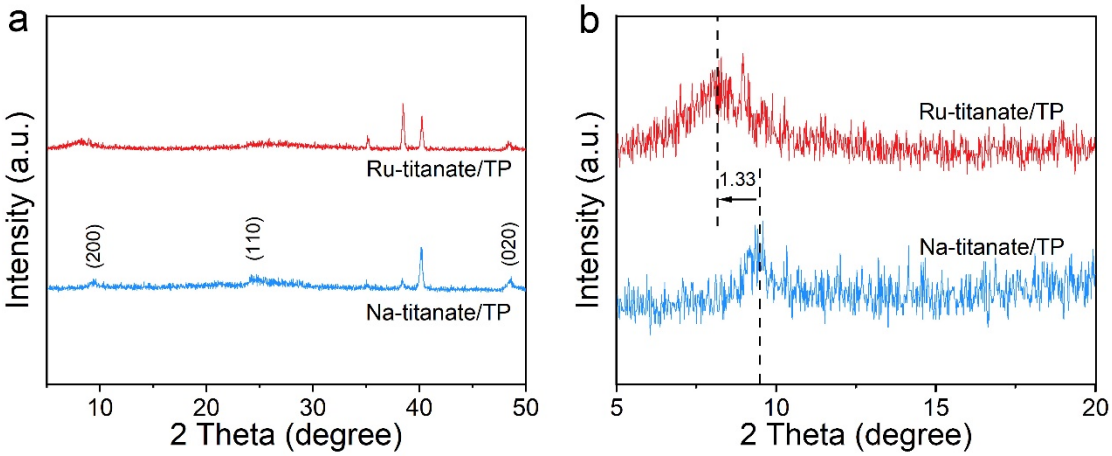

Fig. S2. (a) XRD patterns of Na-titanate/TP and Ru-titanate/TP. (b)The corresponding (200) diffraction peaks shown in an expanded way.

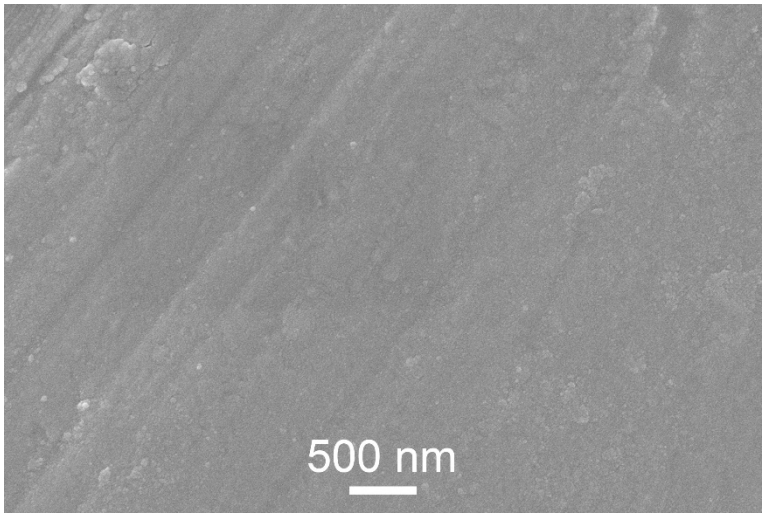

Fig. S3. SEM image of bare TP.

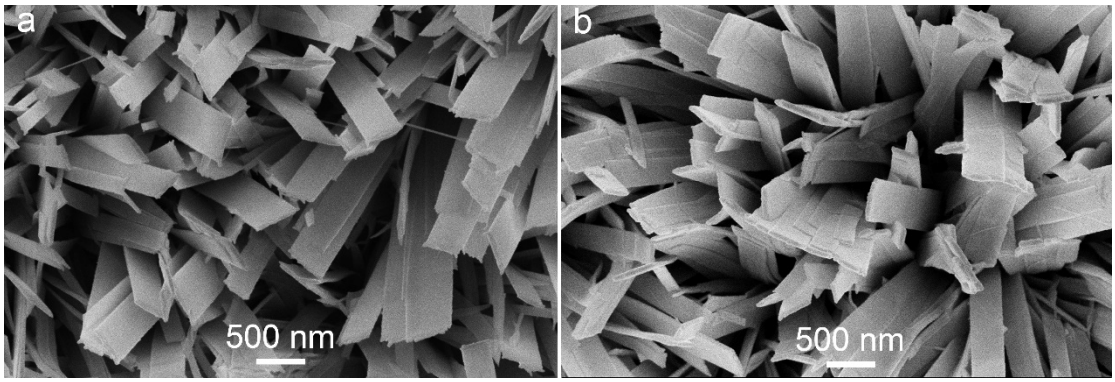

Fig. S4. SEM images of (a) Na-titanate/TP and (b) Ru-titanate/TP.

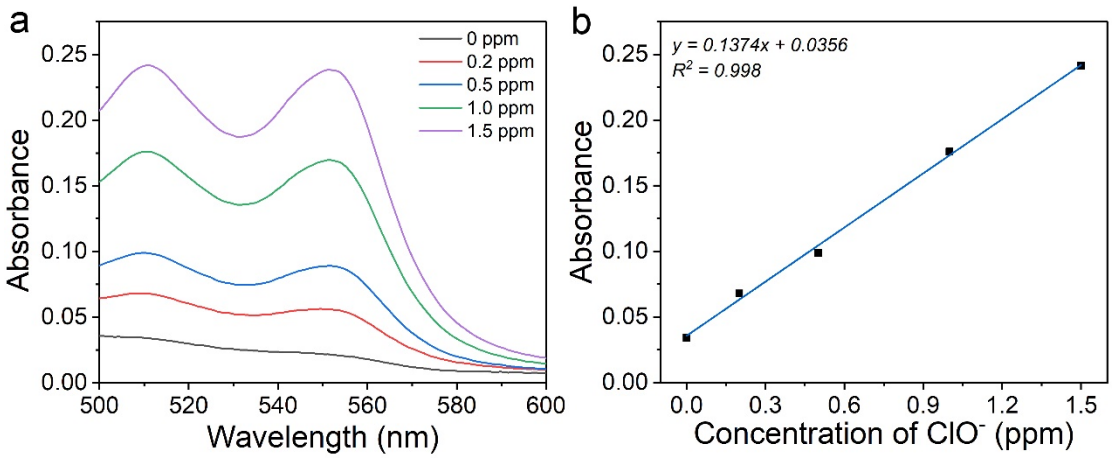

Fig. S5. (a) UV-vis absorption spectra of various active chlorine concentrations at room temperature. (b) Calibration curve used for estimation of active chlorine concentration.

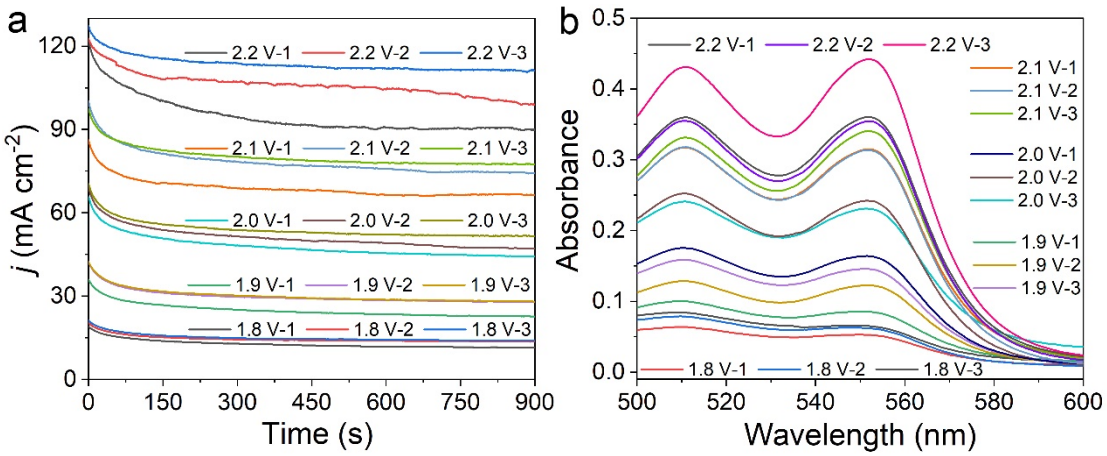

Fig. S6. (a) Chronoamperometry curves and (b) corresponding UV-vis absorption spectra of electrogenerated active chlorine for RuO_2@TiO_2/TP at 1.8 V, 1.9 V, 2.0 V, 2.1 V, and 2.2 V in 0.5 M NaCl + 0.01 M $HClO_4$.

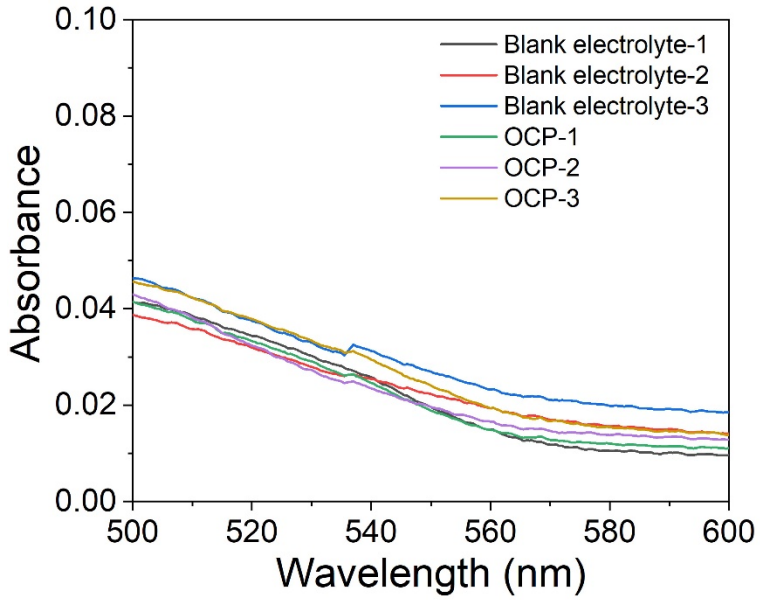

Fig. S7. UV-vis absorption spectra of the electrolytes colored with DPD under different conditions.

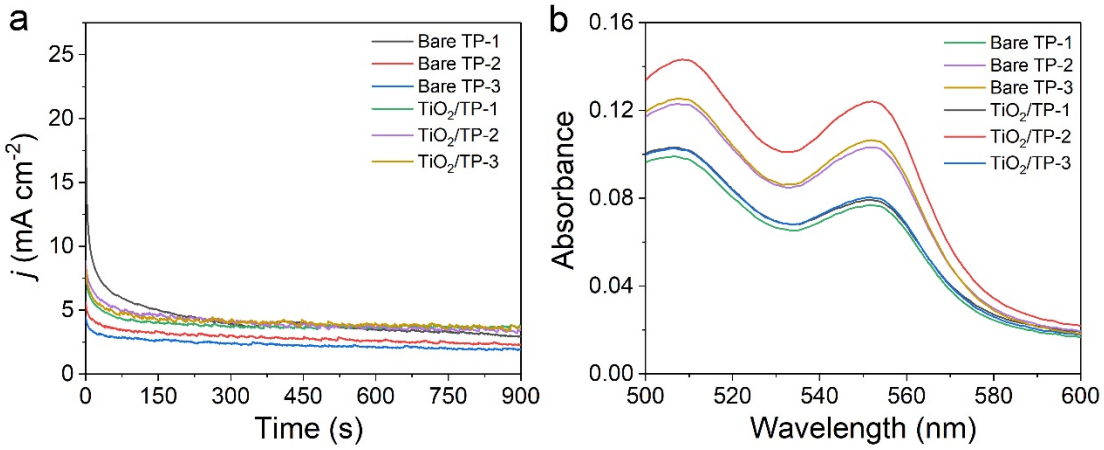

Fig. S8. (a) Chronoamperometry curves for bare TP and TiO_2/TP at 2.1 V and (b) corresponding UV-vis absorption spectra for active chlorine.

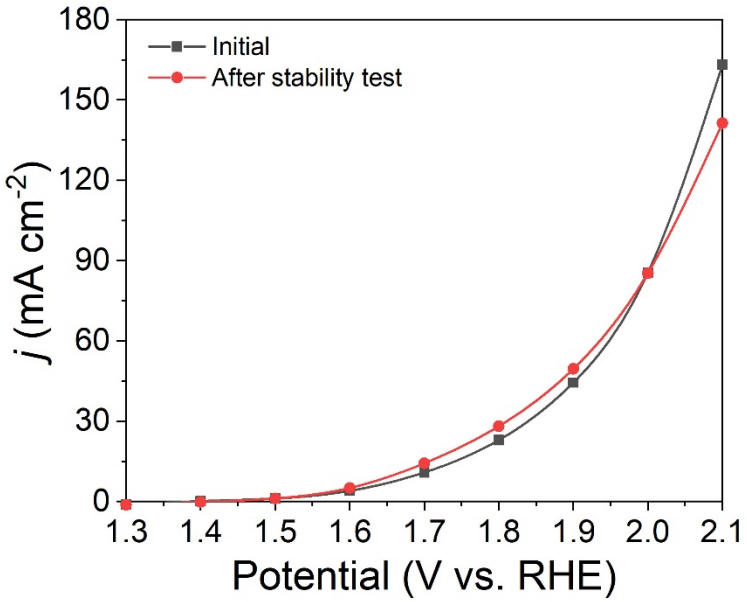

Fig. S9. LSV curves for RuO_2@TiO_2/TP before and after stability test in 0.5 M NaCl + 0.01 M $HClO_4$.

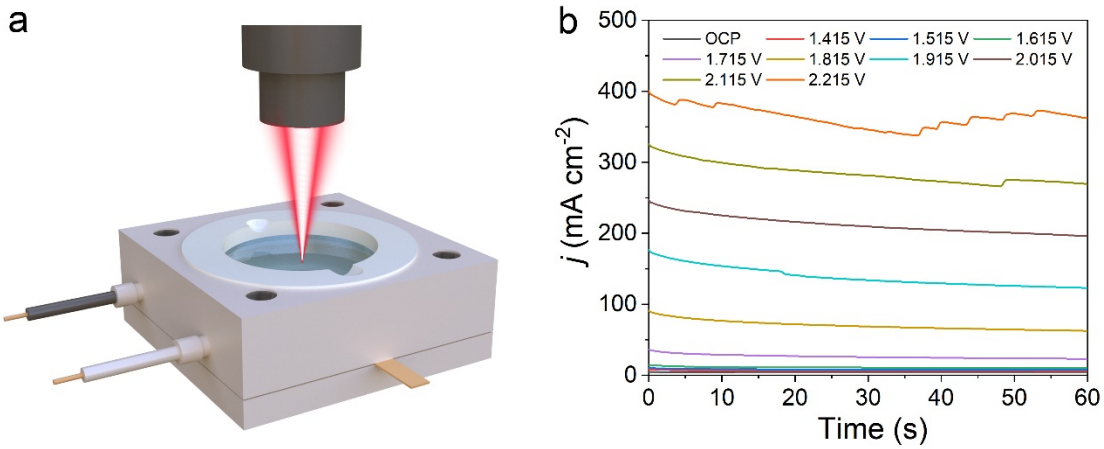

Fig. S10. (a) Schematic of a custom in situ electrochemical Raman cell. (b) Chronoamperometry curves for RuO_2@TiO_2/TP at different potentials in 6 M NaCl + 0.01 M $HClO_4$ for in situ Raman acquisition.

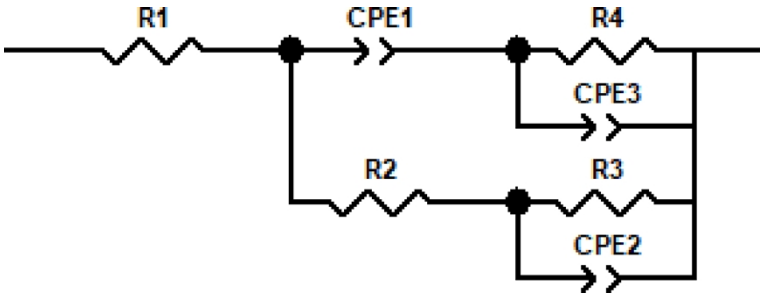

Fig. S11. Electrical equivalent circuit models that may be applicable in aiding the interpretation of the experimental EIS data presented in this article.

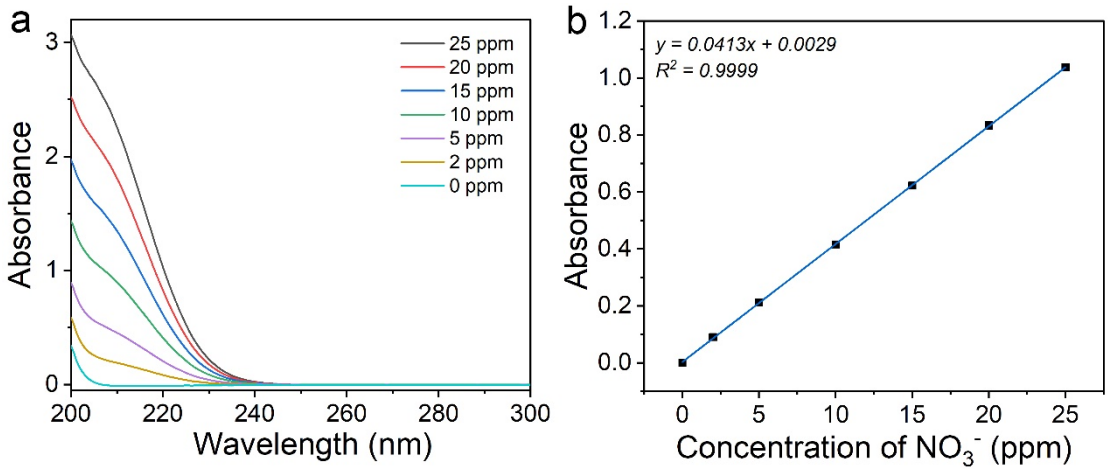

Fig. S12. (a) UV-vis absorption spectra of various nitrate concentrations. (b) Calibration curve used for quantification of nitrate concentration.

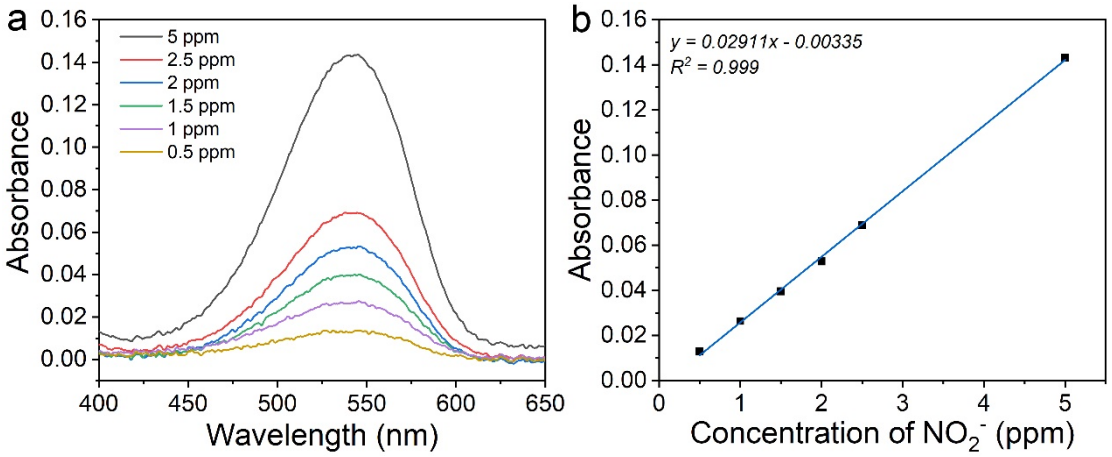

Fig. S13. (a) UV-vis absorption spectra of various nitrite concentrations. (b) Calibration curve used for quantification of nitrite concentration.

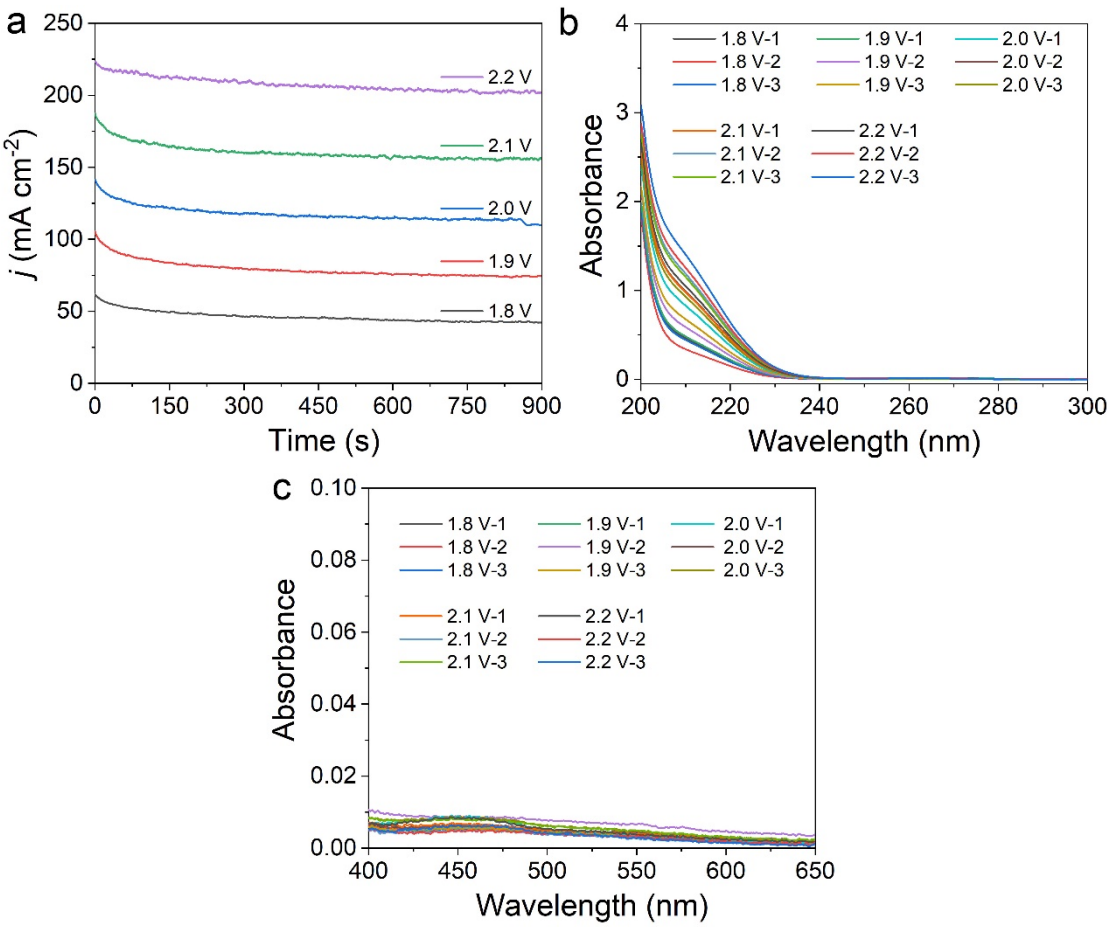

Fig. S14. (a) Chronoamperometry curves and corresponding UV-vis absorption spectra of RuO_2@TiO_2/TP for electrogenerated (b) nitrate and (c) nitrite at 1.8 V, 1.9 V, 2.0 V, 2.1 V, and 2.2 V in NO-saturated 0.5 M NaCl + 0.01 M $HClO_4$.

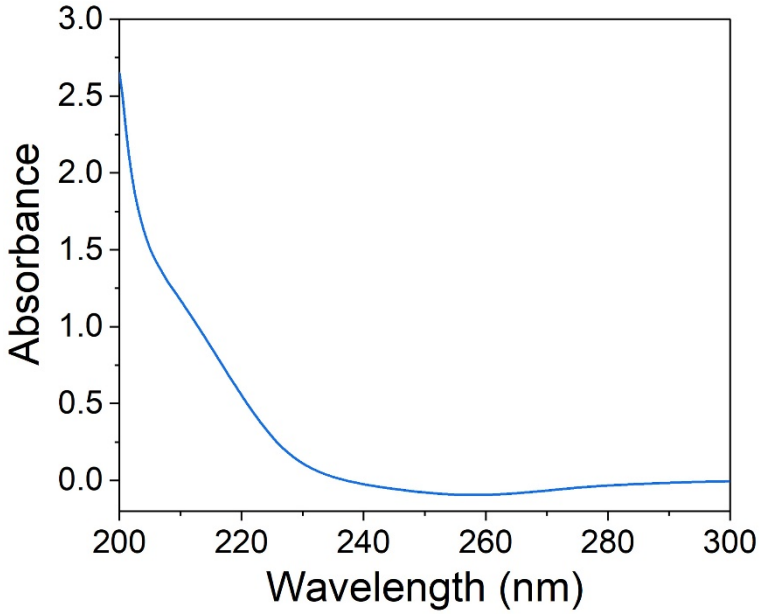

Fig. S15. UV-vis absorption spectra for nitrate in NO and O_2 co-saturated 0.5 M NaCl + 0.01 M $HClO_4$.

We continuously introduced NO and O_2 into 0.5 M NaCl electrolyte containing 0.01 M $HClO_4$ for 30 min, and the nitrate yield in the electrolyte was measured by UV-vis absorption spectroscopy.

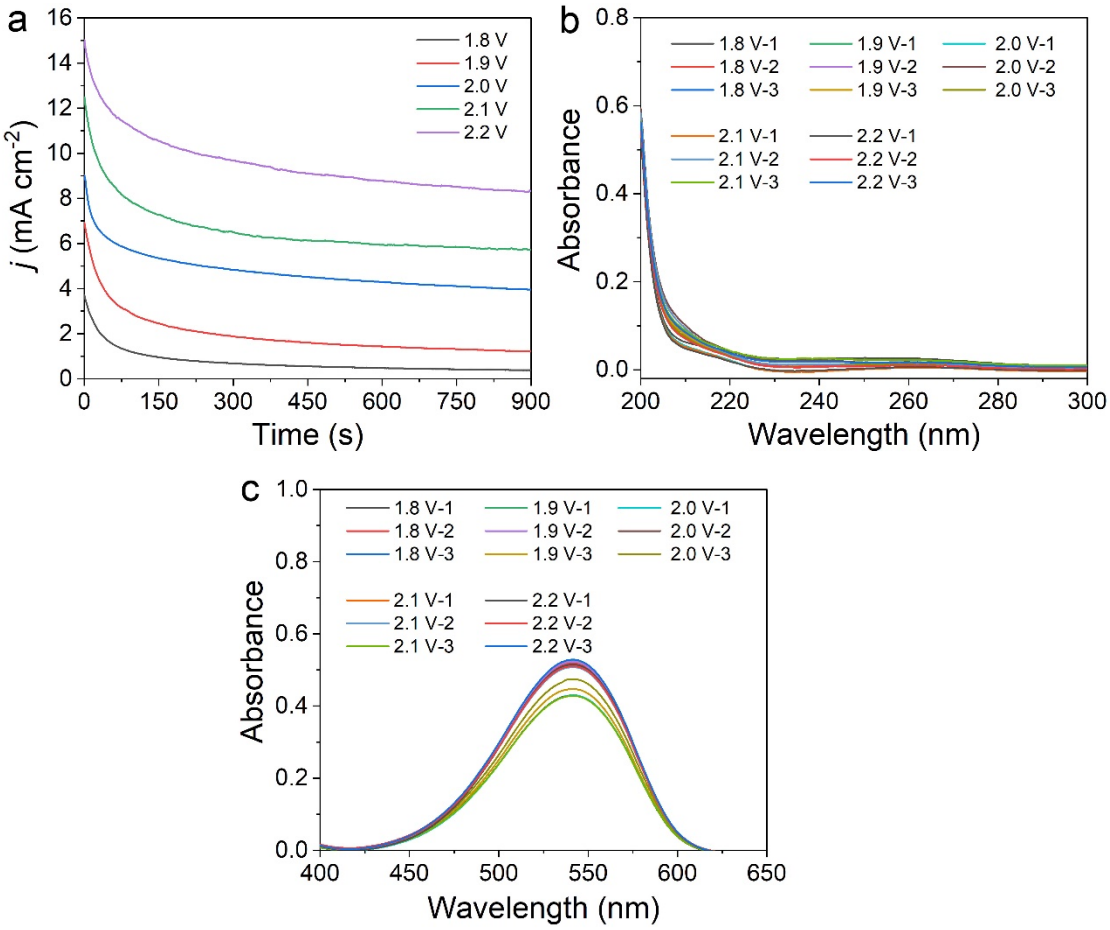

Fig. S16. (a) Chronoamperometry curves and corresponding UV-vis absorption spectra of RuO_2@TiO_2/TP for electrogenerated (b) nitrate and (c) nitrite at 1.8 V, 1.9 V, 2.0 V, 2.1 V, and 2.2 V in NO-saturated 0.5 M Na_2SO_4 + 0.01 M $HClO_4$.

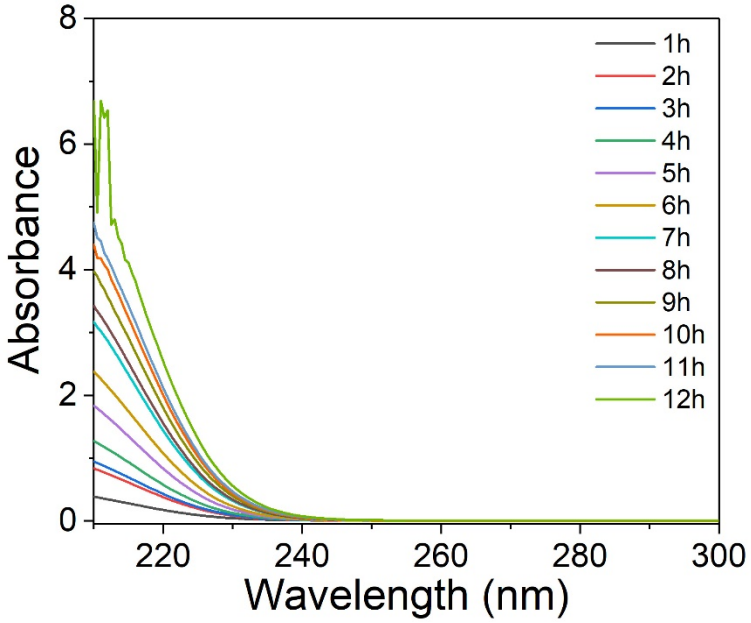

Fig. S17. UV-vis absorption spectra of RuO_2@TiO_2/TP for electrogenerated nitrate in 12-h electrolysis at 2.1 V in NO-saturated 0.5 M NaCl + 0.01 M $HClO_4$.

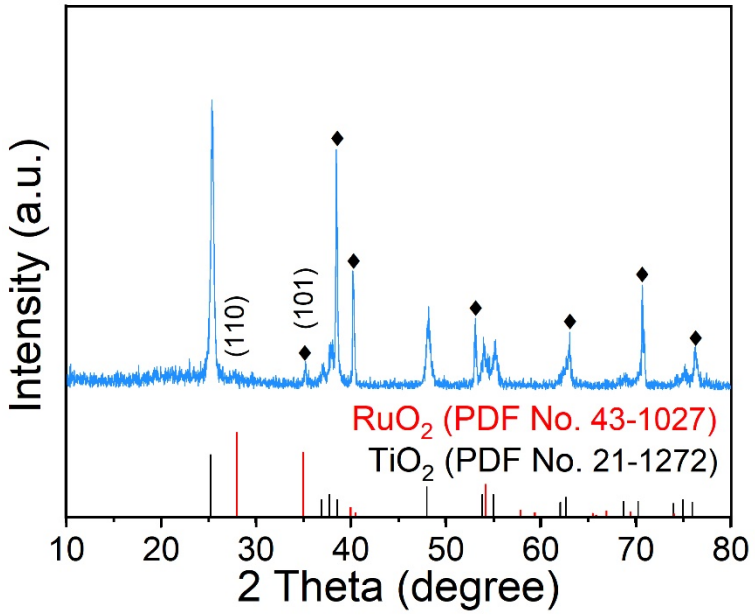

Fig. S18. XRD pattern of RuO_2@TiO_2/TP after stability test in NO-saturated 0.5 M NaCl + 0.01 M $HClO_4$.

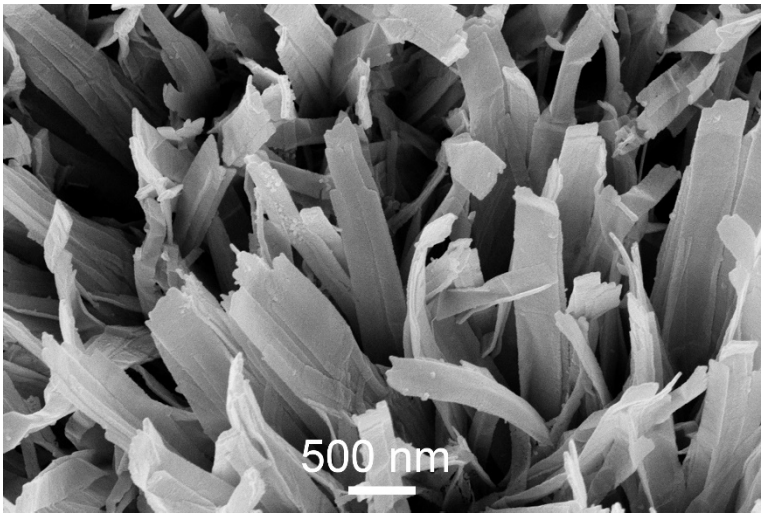

Fig. S19. SEM image of RuO_2@TiO_2/TP after stability test in NO-saturated 0.5 M NaCl + 0.01 M $HClO_4$.

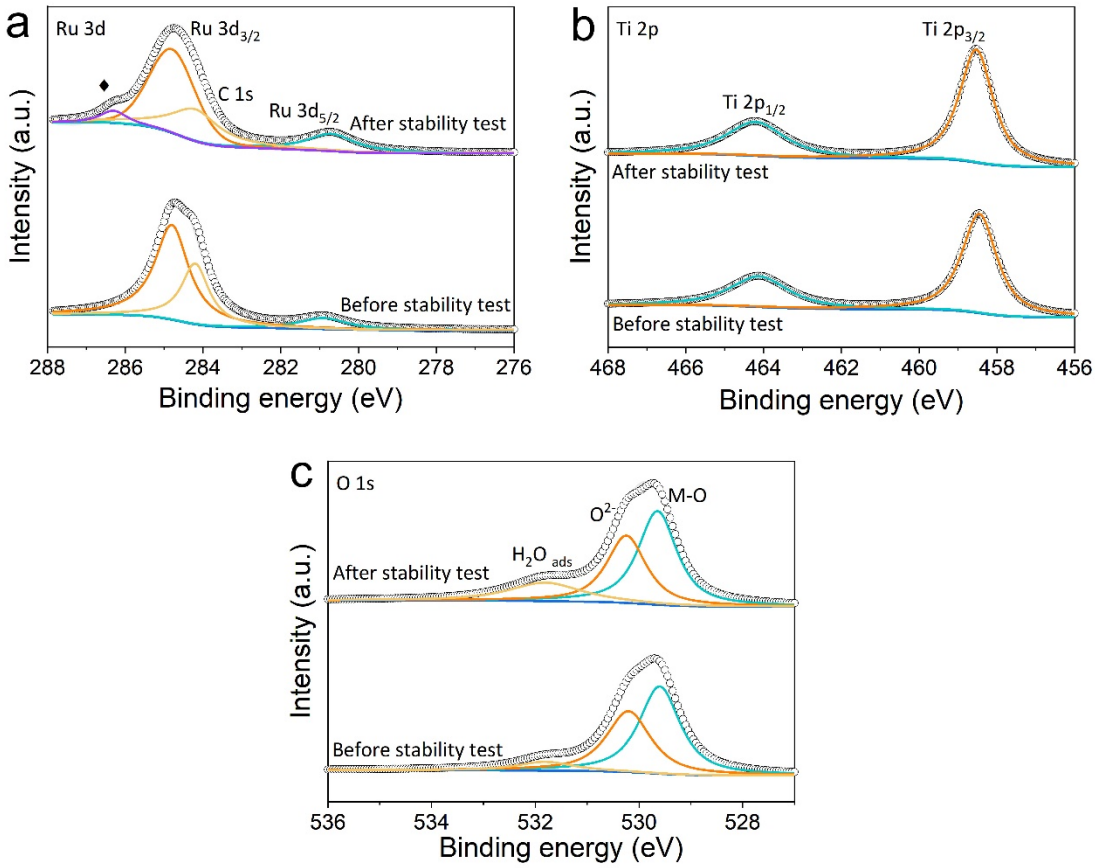

Fig. S20. XPS spectra in the (a) Ru 3d, (b) Ti 2p and, (c) O 1s regions of RuO_2@TiO_2/TP after stability test in NO-saturated 0.5 M NaCl + 0.01 M $HClO_4$.

Table S1. CER electrocatalytic performance comparison of RuO_2@TiO_2/TP with recently reported catalysts.

Electrocatalyst	Electrolyte	Potential	Stability	Reference
RuO_2@TiO_2/TP	0.5 M NaCl + 0.01 M $HClO_4$	1.78 V @ 20 mA cm^{-2}	24 h @ 50 mA cm^{-2}	This work
Ti-Ru-Ir ternary oxide	1 M NaCl	1.90 V @ 10 mA cm^{-2}	/	1
Ti/Sb-SnO_2/Pb_3O_4	0.5 M NaCl	2.36 V @ 10 mA cm^{-2}	/	2
RuO_2-TiO_2	5 M NaCl + 0.001 M $HClO_4$	1.50 V @ 10 mA cm^{-2}	2 h @ 1 A cm^{-2}	3
Sb-doped RuO_2/TNTs	Saturated NaCl	1.81 V @ 10 mA cm^{-2}	/	4
Pt_1/CNT	1 M NaCl + 0.1 M $HClO_4$	1.42 V @ 10 mA cm^{-2}	12 h @ 10 mA cm^{-2}	5
Ru-Ir/TiO_2	4 M NaCl + 0.001 M $HClO_4$	1.65 V @ 10 mA cm^{-2}	/	6
$CoSb_2O_x$	4 M NaCl + 0.01 M HCl	1.71 V @ 10 mA cm^{-2}	90 h @ 100 mA cm^{-2}	7

Table S2. Comparison of nitrate formation rates for RuO_2@TiO_2/TP with recently reported catalysts.

Electrocatalyst	Electrolyte	Nitrate yield	Potential	Reference
RuO_2@TiO_2/TP	0.5 M NaCl + 0.01 M $HClO_4$	95.22 mg cm^{-2} h^{-1}	2.1 V	This work
Ru/TiO_2	0.1 M Na_2SO_4	10.04 μg h^{-1} $mg^{-1}_{cat.}$	2.2 V	8
Ru-Mn_3O_4	0.1 M Na_2SO_4	35.34 μg h^{-1} $mg^{-1}_{cat.}$	2.0 V	9
Fe-SnO_2	0.05 M H_2SO_4	42.9 μg h^{-1} $mg^{-1}_{cat.}$	1.96 V	10
Pd on MXene	0.01 M Na_2SO_4	2.80 μg h^{-1} $mg^{-1}_{cat.}$	2.03 V	11
Au-Nb_2O_{5-x}	4 M NaCl + 0.01 M HCl	2.29 μg $mg^{-1}_{cat.}$ h^{-1}	2.4 V	12
Pd-s PNSs	0.1 M KOH	18.56 μg h^{-1} $mg^{-1}_{cat.}$	1.75 V	13
Platinum foil	0.3 M K_2SO_4	0.06 μmol cm^{-2} h^{-1}	2.19 V	14
Rh NPs	0.1 M KOH + 0.5 M SO_4^{2-}	168 μmol $g_{cat.}^{-1}$ h^{-1}	1.9 V	15
Ru-Doped Pd	0.1 M KOH	77.7 μmol $g_{cat.}^{-1}$ h^{-1}	1.7 V	16
$ZnFe_{0.4}Co_{1.6}O_4$	1 M KOH	130 μmol $g_{cat.}^{-1}$ h^{-1}	1.6 V	17

References

(1) G. A. R. Zeradjanin, N. Menzel, W. Schuhmann and P. Strasser, On the faradaic selectivity and the role of surface inhomogeneity during the chlorine evolution reaction on ternary Ti-Ru-Ir mixed metal oxide electrocatalysts, *Phys. Chem. Chem. Phys.,* 2014, **16**, 13741–13747.

(2) D. Shao, W. Yan, L. Cao, X. Li and H. Xu, High-performance Ti/Sb-SnO_2/Pb_3O_4 electrodes for chlorine evolution: preparation and characteristics, *J. Hazard. Mater.,* 2014, **267**, 238–244.

(3) K. Xiong, L. Peng, Y. Wang, L. Liu, Z. Deng, L. Li and Z. Wei, In situ growth of RuO_2-TiO_2 catalyst with flower-like morphologies on the Ti substrate as a binder-free integrated anode for chlorine evolution, *J. Appl. Electrochem.,* 2016, **46**, 841–849.

(4) H. Cao, D. Lu, J. Lin, Q. Ye, J. Wu and G. Zheng, Novel Sb-doped ruthenium oxide electrode with ordered nanotube structure and its electrocatalytic activity toward chlorine evolution, *Electrochim. Acta,* 2013, **91**, 234–239.

(5) T. Lim, G. Y. Jung, J. H. Kim, S. O. Park, J. Park, Y.-T. Kim, S. J. Kang, H. Y. Jeong, S. K. Kwak and S. H. Joo, Atomically dispersed Pt-N_4 sites as efficient and selective electrocatalysts for the chlorine evolution reaction, *Nat. Commun.,* 2020, **11**, 412.

(6) N. Menzel, E. Ortel, K. Mette, R. Kraehnert and P. Strasser, Dimensionally stable Ru/Ir/TiO_2-anodes with tailored mesoporosity for efficient electrochemical chlorine evolution, *ACS Catal.,* 2013, **3**, 1324–1333.

(7) I. A. Moreno-Hernandez, B. S. Brunschwig and N. S. Lewis, Crystalline nickel, cobalt, and manganese antimonates as electrocatalysts for the chlorine evolution reaction, *Energy Environ. Sci.,* 2019, **12**, 1241–1248.

(8) M. Kuang, Y. Wang, W. Fang, H. Tan, M. Chen, J. Yao, C. Liu, J. Xu, K. Zhou and Q. Yan, Efficient nitrate synthesis via ambient nitrogen oxidation with Ru-doped TiO_2/RuO_2 electrocatalysts, *Adv. Mater.,* 2020, **32**, 2002189.

(9) Z. Nie, L. Zhang, X. Ding, M. Cong, F. Xu, L. Ma, M. Guo, M. Li and L. Zhang, Catalytic kinetics regulation for enhanced electrochemical nitrogen oxidation by Ru-nanoclusters-coupled Mn_3O_4 catalysts decorated with atomically dispersed Ru atoms, *Adv. Mater.,* 2022, **34**, 2108180.

(10) L. Zhang, M. Cong, X. Ding, Y. Jin, F. Xu, Y. Wang, L. Chen and L. Zhang, A janus Fe-SnO_2 catalyst that enables bifunctional electrochemical nitrogen fixation, *Angew. Chem., Int. Ed.,* 2020, **59**, 10888–10893.

(11) W. Fang, C. Du, M. Kuang, M. Chen, W. Huang, H. Ren, J. Xu, A. Feldhoff and Q. Yan, Boosting efficient ambient nitrogen oxidation by a well-dispersed Pd on MXene electrocatalyst, *Chem. Commun.,* 2020, **56**, 5779–5782.

(12) Y. Zhang, F. Du, R. Wang, X. Ling, X. Wang, Q. Shen, Y. Xiong, T. Li, Y. Zhou and Z. Zou, Electrocatalytic fixation of N_2 into NO_3^-: electron transfer between oxygen vacancies and loaded Au in Nb_2O_{5-x} nanobelts to promote ambient nitrogen oxidation, *J. Mater. Chem. A,* 2021, **9**, 17442−17450.

(13) S. Han, C. Wang, Y. Wang, Y. Yu and B. Zhang, Electrosynthesis of nitrate via the oxidation of nitrogen on tensile-strained palladium porous nanosheets, *Angew. Chem., Int. Ed.,* 2021, **60**, 4474−4478.

(14) Y. Wang, Y. Yu, R. Jia, C. Zhang and B. Zhang, Electrochemical synthesis of nitric acid from air and ammonia through waste utilization, *Natl. Sci. Rev.,* 2019, **6**, 730−738.

(15) T. Li, S. Han, C. Cheng, Y. Wang, X. Du, Y. Yu and B. Zhang, Sulfate-enabled nitrate synthesis from nitrogen electrooxidation on a rhodium electrocatalyst, *Angew. Chem., Int. Ed.,* 2022, **61**, e202204541.

(16) T. Li, S. Han, C. Wang, Y. Huang, Y. Wang, Y. Yu and B. Zhang, Ru-doped Pd nanoparticles for nitrogen electrooxidation to nitrate, *ACS Catal.,* 2021, **11**, 14032−14037.

(17) C. Dai, Y. Sun, G. Chen, A. C. Fisher and Z. J. Xu, Electrochemical oxidation of nitrogen towards direct nitrate production on spinel oxides, *Angew. Chem., Int. Ed.,* 2020, **59**, 9418−9422.